Noise performance of diffusion cooled hot-electron bolometers: theory vs. experiment

P.J. Burke, R.J. Schoelkopf, I. Siddiqi, and D.E. Prober
Departments of Applied Physics and Physics, Yale University, 15 Prospect St., New Haven, CT 06520-8284

A. Skalare, B.S. Karasik, M.C. Gaidis, W.R. McGrath, B.Bumble, and H.G. LeDuc
Center for Space Microelectronics Technology, Jet Propulsion Laboratory, Caltech, Pasadena, CA 91109

We have measured the spectrum of the output noise and the conversion gain from 0.1-7.5 GHz under identical conditions for both diffusion and phonon-cooled Nb bolometers, using a 20 GHz LO on a variety of devices varying in length from 0.08 μm to 3 μm, where the gain-bandwidth varies between 100 MHz and > 6 GHz. In this paper, we will present systematic comparison between theory and experiment for the devices measured. We find the frequency dependence of the device conversion efficiency and noise is well described by a simple thermal model. We have used two methods of inferring dR/dT, and describe the predictions for the magnitude of the efficiency and noise based on these. Neither method provides consistent quantitative predictions of the magnitude of device performance for a variety of operating conditions. Thus the device performance, while excellent, must continue to be investigated experimentally. We have therefore begun a series of experiments on lower T_c devices made of Al, which may have improved performance.

I. INTRODUCTION

Recent research on hot-electron bolometer mixers has enhanced the prospect of acheiving quantum-noise-limited performance ($T_Q = h\nu/k$) in heterodyne receivers at THz frequencies. Hot-electron bolometer mixers of both the phonon cooled [1] and diffusion cooled [2–4] type have already shown excellent noise performance. We have recently predicted [5] and shown [2,6] that for Nb devices diffusion cooling provides much larger intermediate frequency (IF) gain bandwidth than can be obtained with phonon cooling, due to faster thermal response. We have also recently shown [7–9] that the spectrum of the device output noise obeys a simple thermal model, consisting of frequency-dependent thermal flucuation noise plus a white background (Johnson noise). There, it was shown that there is a frequency scale associated with the dominant part of the output noise that scales with device length as it does for the gain bandwidth. In this paper, we present detailed comparisons of the zero IF magnitude of the conversion efficiency and output noise with theoretical predictions.

II. THEORY

For a lumped thermal element, theoretical calculations have already been performed which relate the device conversion efficiency and output noise to the dc current, LO power, device resistance, thermal conductance, temperature, and change of resistance with temperature (dR/dT) [10–12]. In this section, these lumped-element calculations are summarized in order to allow comparison with theory. A diffusion cooled device should properly be modeled as

a distributed thermal system. The results of our calculations for the distributed system are given later in this section and related to the lumped element approach calculations already available in the literature. A more microscopic approach which treats the spatial distribution of the superconducting energy gap in the presence of strong ac and dc self-heating, such as that being developed in [13], is desirable. We use the normal state heating results as a guide until a more complete theory can be developed.

A. Lumped Element Predictions

1. Conversion efficiency

The coupled conversion efficiency, defined as the power out at the IF over the power in at the rf, can be predicted in terms of the dc current I_{dc}, the LO power P_{LO}, the thermal conductance to the bath G, the resistance $R \equiv V_{dc}/I_{dc}$, and the change in resistance with temperature dR/dT as [10–12]

$$\eta(\omega) = \eta_{IF}\frac{P_{LO}}{2\,R}\left(\frac{I_{dc}(dR/dT)}{G_{eff}}\right)^2\frac{1}{1+(\omega\tau_{eff})^2} \tag{1}$$

$$= \eta(0)\frac{1}{1+(\omega\tau_{eff})^2}, \tag{2}$$

where ω is the IF. This is the single-sideband (SSB) efficiency. We define the "gain bandwidth" as the IF at which the conversion efficiency drops be 3 dB relative to its low IF value. Thus, from Eq. 1, the gain bandwidth is given by $f_{3dB,gain} = 1/(2\pi\tau_{eff})$. Here τ_{eff} is the effective thermal time constant and G_{eff} the effective thermal conductance to the bath. The effective thermal conductance and time constant are related to the "bare" thermal conductance G and time constant τ_{th} by

$$\tau_{eff} \equiv \tau_{th}/(1-\alpha), \tag{3}$$

$$\tau_{th} \equiv C/G, \tag{4}$$

$$G_{eff} \equiv G\,(1-\alpha), \tag{5}$$

$$\alpha \equiv \frac{I_{dc}^2 dR/dT}{G}\left(\frac{R_L-R}{R_L+R}\right) \tag{6}$$

$$= \alpha_0\left(\frac{R_L-R}{R_L+R}\right) \tag{7}$$

$$\alpha_0 \equiv \frac{I_{dc}^2 dR/dT}{G}, \tag{8}$$

where C is the (electronic) heat capacity, and R_L the load resistance at the IF, i.e., the input resistance of the IF amplifier, which is typically 50 Ω. The effect of the electro-thermal feedback between the electron temperature and the dc bias supply is described quantitatively by the parameter α. If α is small (due to small current or small dR/dT), then the effect of electro-thermal feedback is small, and the effective time constant τ_{eff} is equal to the "bare" thermal time constant τ_{th}, and the effective thermal conductance G_{eff} is equal to the bare thermal conductance G. The IF load resistance tends to suppress electro-thermal feedback if the device resistance R is comparable to the load resistance R_L. This is the case for the devices studied in this work.

The factor η_{IF} is defined as

$$\eta_{IF} \equiv \frac{4RR_L}{(R+R_L)^2}, \tag{9}$$

where R_L is the IF load resistance. This factor is not a standard mismatch factor in the usual sense, since the device impedance depends on frequency, whereas Eq. 9 is independent of frequency. The factor results from a more rigorous calculation of the effect of a finite load impedance at the IF on the electron dynamics [10,12]. The parameter varies between zero and one, and is one when the device resistance is equal to the input impedance of the IF amplifier.

2. Output Noise

In hot-electron bolometers, the important noise sources are expected to be thermal fluctuation noise and Johnson noise. The prediction for the output noise due to thermal fluctuations T_{TF} is given by [10–12]:

$$T_{TF}(\omega) = \left(I_{dc}T_e(dR/dT)\right)^2 \frac{1}{RG_{eff}(1-\alpha)} \frac{1}{1+(\omega\tau_{eff})^2}\ \eta_{IF} \tag{10}$$

$$= T_{TF}(0)\frac{1}{1+(\omega\tau_{eff})^2}, \tag{11}$$

where η_{IF} is the IF mismatch factor in Eq. 9, and T_e the electron temperature.

In addition to affecting the thermal fluctuation noise, electro-thermal feedback also affects the Johnson noise. The resultant expression for the Johnson output noise is given by [14,12]:

$$T_{John} = T_e\ \frac{1}{(1-\alpha)^2}\ \left(\frac{1+(\omega\tau_{th})^2}{1+(\omega\tau_{eff})^2}\right)\ \eta_{IF}. \tag{12}$$

This should be added to T_{TF} to get the total output noise, i.e.

$$T_{out}(\omega) = T_{John} + \frac{T_{TF}(0)}{1+(\omega\tau_{eff})^2} \tag{13}$$

3. Mixer noise

The single-sideband (SSB) *mixer noise* $T_{mix} \equiv T_{out}/\eta$ is the noise referred to the input. (The double-sideband mixer noise is one half of the SSB mixer noise.) The mixer noise can now be calculated on the basis of the above calculations. The result is [12]:

$$T_{mix}(\omega)(SSB) = \frac{2T_e^2G}{P_{LO}} + \frac{2RT_eG^2}{P_{LO}I_{dc}^2(dR/dT)^2}\left(1+(\omega\tau_{eff})^2\right). \tag{14}$$

The first term is due to the thermal fluctuation noise, while the second term is due to the Johnson noise. The second term is dependent on the IF. This is simply due to that fact that Johnson noise is white, whereas the conversion efficiency decreases as the IF is increased. As a result of this, the *gain bandwidth* (i.e., the IF at which the conversion efficiency drops

by 3 dB) is not necessarily equal to the *noise bandwidth*, $f_{3dB,noise}$, which we define as the frequency at which the *mixer noise* increases by a factor of two. In fact, using Eq. 14, it is simple to show that [15]:

$$\frac{f_{3dB,noise}}{f_{3dB,gain}} = \sqrt{\frac{T_{John} + T_{TF}(0)}{T_{John}}}. \tag{15}$$

B. Distributed system predictions

For a distributed non-superconducting system, the output noise temperature due to Johnson noise is predicted to be the average temperature along the length of the bridge. However, a quantitative theory for the conversion efficiency and thermal fluctuation noise which treats the device as a distributed system has not yet been developed[1]. Therefore, in this section we will take the average temperature to determine the Johnson noise. We calculate the temperature profile under conditions of uniform dissipation of dc and ac power and attempt to relate the distributed system approach to the lumped element approach by deriving an effective time constant and thermal conductance between the electrons and the bath. These quantities can then be used in the theory of section II A as an approximation to expected device performance.

The impedance of the device at frequencies above the energy gap frequency ($\approx$ 700 GHz in bulk Nb) is constant and equal to the normal state impedance. Therefore, if a high frequency signal is applied above the energy gap frequency, then the dissipation of power *is* uniform. However, if the frequency of the applied signal is less than the energy gap frequency, then it is possible that the dissipation of power varies spatially, since the temperature and hence resistance vary spatially. At T_c the energy gap vanishes, suggesting that the dissipation of power may still be uniform at all frequencies.

1. DC heating, no electron-phonon interaction

In the steady state, the flow of heat and the electron temperature are governed by the time-independent heat-diffusion equation. It can be shown [16,17] that the electron temperature along the length of the device is given by

$$T_e(x) = T_b\sqrt{1 + \frac{x}{L}\left(1 - \frac{x}{L}\right)\frac{PR}{T^2\mathcal{L}}}. \tag{16}$$

Here P is the power dissipated, T_b the bath temperature, and $\mathcal{L}$ the Lorenz number. The temperature profile is not directly measured in this work. To relate the above calculation more directly to measurements, we need to calculate the average temperature rise as a function of input power. The result is [18,17]:

---

[1]The case of a lumped element connected to a bath *through* a distributed system was considered in [14] and [12].

$$< T_e >= \frac{T_b}{2} + \left[T_b^2\sqrt{\frac{\mathcal{L}}{PR}} + \frac{1}{4}\sqrt{\frac{PR}{\mathcal{L}}}\right] \arcsin\left(\sqrt{\frac{PR}{4T_b^2\mathcal{L} + RP}}\right) \tag{17}$$

2. AC heating, no electron-phonon interaction

When the source of heating is time-dependent, as in most of the experiments in this work, the equation that governs the temperature profile is the time-dependent generalization of the heat diffusion equation. We have solved for the electron temperature $T_e(x,t)$ and find for a time dependent input power given by $P(t) = P_0 + P_\omega e^{i\omega t}$ that the electron temperature averaged along the length of the device is given by:

$$< T_e(x,t) >_x = T_b + P_0 \frac{\frac{L^2}{12D}}{C} + e^{i\omega t} P_\omega \frac{8}{\pi^2}\frac{\tau_0}{C}\sum_{n=0}^{+\infty}\frac{1}{(2n+1)^4}\frac{1}{1+i\omega\tau_n}, \tag{18}$$

where C is the heat capacity (the specific heat c times the volume), and τ_n is defined as

$$\tau_n \equiv \frac{L^2}{\pi^2 D(2n+1)^2}; \tag{19}$$

the diffusion constant D is equal to the thermal conductivity K divided by the specific heat c. The second term in Eq. 18 simply gives the dc rise in the average temperature. This allows a dc thermal conductance to be calculated from

$$< T_e >_x = \frac{P_0}{C/\frac{L^2}{12D}} = \frac{P_0}{\mathcal{L}T_b/\frac{R}{12}}. \tag{20}$$

Thus, the resultant "effective" dc thermal conductance is given by

$$G = \frac{\mathcal{L}T_b}{R/12}. \tag{21}$$

(This results in an effective resistance of $R/12$ derived by one of us in [5].) The third term in Eq. 18 is the ac component of the average temperature rise. To a good approximation, a lumped element approach can still be used, provided an effective thermal time constant of

$$\tau_{th} = \frac{L^2}{\pi^2 D} \tag{22}$$

is used. This time constant is *not* equal to the heat capacity C divided by the dc thermal conductance G, defined in Eq. 21. (Ref. [5] had used $\tau_{th} = C/G$; we now see that choice was in error by $\sim$ 20%. We choose to express the results in this work in terms of R/12, since that quantity was defined as "$R_{effective}$" in ref. [5].) The diffusion time constant is equal to τ_{e-ph} when the bridge length is equal to πL_{e-ph}. Therefore, the crossover from phonon-cooled to diffusion-cooled behavior occurs at $L = \pi L_{e-ph}$.

3. Spatially distributed temperature fluctuations, no electron-phonon interaction

In section II A 2, the fluctuations in the temperature of a single thermal element connected through a thermal conductance to the thermal bath were considered. In a distributed system, fluctuations in the flow between nearest neighbors are postulated, and the magnitude of forcing function must be calculated. A generalized Langevin equation can be derived [19–21] for this process. In this work, we consider the solution to that equation with boundary conditions that the temperature at the ends is fixed. We find the following for the resultant spectral density of the temperature fluctuations:

$$\Big(< \delta T_e(x,\omega) >_x\Big)^2 = \frac{4k_B T_e^2}{\frac{\tau_0}{C}\frac{\pi^2}{8}} \sum_{n=0}^{+\infty} \frac{1}{(2n+1)^4} \frac{1}{1+(\omega\tau_n)^2}. \tag{23}$$

This equation was derived when no external power is applied, so that T_e is well defined, and equal to the bath temperature. The first term in Eq. 23 is the dominant term, and so the lumped element approximation can still be used to a very good approximation, provided an effective thermal time constant given by Eq. 22 is used. Finally, the low-frequency limit of Eq. 23 is:

$$\lim_{\omega\to 0}\Big(< \delta T_e(x,\omega) >_x\Big)^2 = \frac{4k_B T_e^2}{C/\frac{L^2}{12D}} = \frac{4k_B T_e^2}{\mathcal{L}T_b/\frac{R}{12}}. \tag{24}$$

Thus, the lumped element prediction for the thermal fluctuation noise (eq. 10) can be used, provided the dc effective thermal conductance of $\mathcal{L}T_b/\frac{R}{12}$ (eq. 21) is used.

4. DC heating with electron-phonon interaction

In the presence of electron-phonon interaction, the diffusion equation contains a "sink" term for the heat flow: power can flow from the electron system directly to the phonon system. The power flow density depends on the electron temperature and the phonon temperature, as well as the electron mean-free-path. There is no theoretical prediction that accounts for the strength of the electron-phonon coupling in Nb, so empirical results must be used. Experimentally [22], the electron-phonon coupling is given by:

$$p_{out} = A(T_e^4 - T_{ph}^4), \tag{25}$$

where p_{out} is the electron-phonon power flow per unit volume, and $A = 1 - 2\text{x}10^{10}\ W\ m^{-3}\ K^{-4}$ for D = 1 cm^2/s.

5. AC heating in the presence of electron phonon interaction; strong AC heating

Based on the above results, we can come to the following conclusions regarding the temperature profile: For very long devices, in the presence of weak or strong dc or ac heating, the behavior should be that of a lumped element with a single time constant, τ_{e-ph}. For devices much shorter than πL_{e-ph} in the presence of weak ac heating, a lumped element is a good approximation, with a single time constant of $L^2/\pi^2 D$. A similar conclusion is expected to hold in the case of strong ac heating, without electron-phonon interactions; this has not yet been calculated. A numerical calculation of the time-dependent diffusion

equation in the presence of electron-phonon interactions would be required to quantitatively evaluate the behavior between the two regimes. However, we expect that the cooling rates should approximately add, and this approximation will be used in the remainder of this paper.

C. Voltage dependence of conversion efficiency and noise; α from I-V curve

When dc and ac power are applied to the device, the electron temperature is heated above the bath temperature to somewhere near the critical temperature. However, the temperature of the electron system is difficult to predict accurately. This makes predictions of the conversion efficiency and output noise difficult, since dR/dT depends sensitively on the electron temperature near T_c. There is, however, a way to determine the value of α from the measured I-V curve which allows predictions of the output noise and efficiency. An increase in bias voltage increases the power dissipated, which raises the electron temperature. This in turn causes an increase in resistance. Based on this physical principle, a derivation is given in [11] for the following formula:

$$I_{dc}^2 dR/dP = I_{dc}^2 (dR/dT)/G = \frac{(dV/dI) - R}{(dV/dI) + R} \equiv \alpha_0. \tag{26}$$

Therefore, the measured dc I-V curve can provide a measurement of α_0. (It is straightforward to calculate α from the dc I-V curve once α_0 is known.) The predictions of Eqs. 1 and 10 can be rewritten in terms of α and α_0 as

$$\eta(\omega_{IF}) = \frac{P_{LO}}{2\ P_{dc}} \frac{\alpha_0^2}{(1-\alpha)^2} \frac{1}{1+(\omega_{IF}\tau_{eff})^2} \eta_{IF}, \tag{27}$$

$$T_{out} = \frac{T_e^2\ G}{P_{dc}} \frac{\alpha_0^2}{(1-\alpha)^2} \frac{1}{1+(\omega_{IF}\tau_{eff})^2}\ \eta_{IF}. \tag{28}$$

The values of P_{dc}, P_{LO}, G, and T_e can be estimated with reasonable accuracy, so a prediction of device performance from the measured I-V curve is possible.

III. EXPERIMENTAL TECHNIQUE

A. Device Fabrication

The devices studied were all fabricated from the same thin (100 Å) Nb film, deposited on a quartz substrate. The patterned film has a transition temperature of $T_c \approx 5$ K, transition width $\Delta T_c \sim 0.5K$, and sheet resistance $\approx$ 33 Ω. The length of the bridge was defined by the normal metal (1000 Å thick Au) contacts using direct write e-beam lithography in a self-aligned process [23]. The length and width of the devices measured in this work were determined by inspecting the SEM image of different devices with the same design length in the same fabrication run. The estimated error using this technique is approximately ± 0.05 μm. The devices measured in this work were not measured in an SEM, in order to avoid electrical damage. The device dc properties are summarized in Table I. The measured resistance vs. temperature curves are plotted in Fig. 1.

TABLE I. Device geometries and dc resistances.

Device:	Length (μm)	Width (μm)	R_N (Ω)	dR/dT[a] (Ω/K)
A1	0.08	0.08	56	140
A2	0.08	0.08	56	-
B	0.16	0.08	80	200
C	0.24	0.08	96	250
D	0.6	0.2	93	-
E	3	1	86	-

[a]For this table, dR/dT is evaluated at the steepest point on the R vs. T curve.

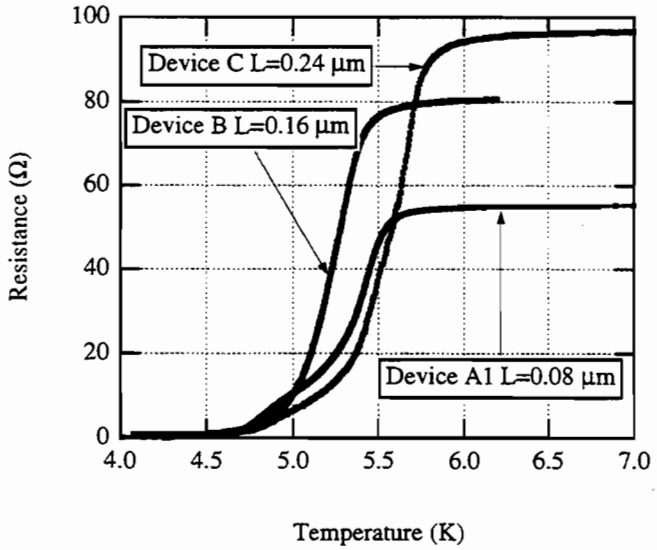

FIG. 1. Resistance vs. temperature curves for diffusion-cooled devices.

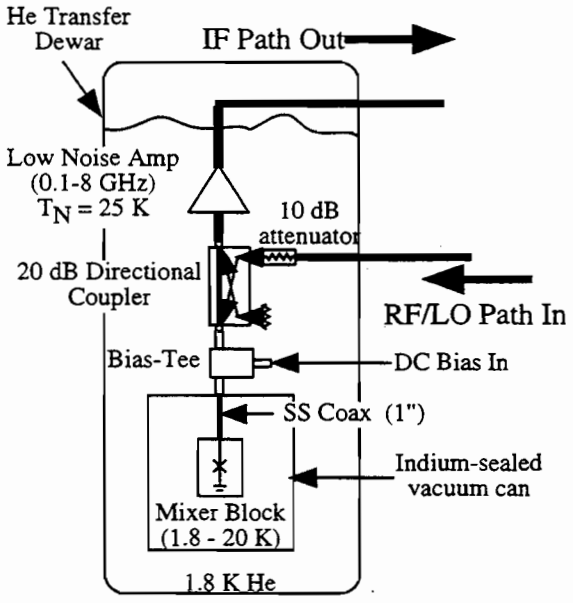

FIG. 2. Schematic of experimental setup.

B. Measurement technique and calibrations

Each device was mounted at the end of a section of 50 Ω microstrip, using a "flip-chip" configuration to assure a broadband match. A cooled directional coupler was used to weakly couple in the rf and LO. The through port was connected to a cooled, low noise ($\approx$ 25 K), broadband amplifier. The cable losses, amplifier gain, and coupler performance were each measured at 2 K. The mixer conversion efficiency as a function of intermediate frequency was thus measured to ± 2 dB. The amplifier chain noise and gain were calibrated *in-situ* to the plane of the device by heating the device above T_c and using it as a variable temperature load. This calibration applies for a source impedance given by R_n. Some measurements were performed with an isolator to confirm that impedance mismatch effects were not significantly affecting the calibration. Additional measurements of the return loss of the devices were performed in order to determine the impedance mismatch in the intermediate state. The coupling was 90% or better over the frequency range measured for all the devices, except device E. Therefore, the lack of an isolator should not significantly modify the calibration constants of the amplifier gain and noise which were determined when the device was in the normal state. A schematic of the experimental setup is shown in Fig. 2.

IV. EXPERIMENTAL RESULTS

A. Conversion efficiency and Noise

The measured conversion efficiency, output noise, and mixer noise all depend on several parameters under experimental control for a given device. We first discuss the dependence

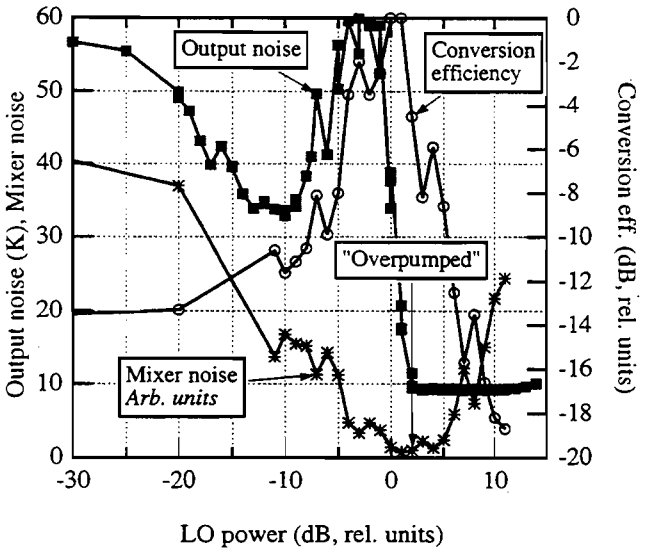

FIG. 3. Efficiency, output noise, and mixer noise vs. LO power for device A1.

on LO power, then on dc power, then on the IF. The measurements of the conversion efficiency and noise were all performed at a bath temperature of 2 K.

1. Conversion efficiency and noise vs. LO power

The (relative) conversion efficiency, output noise, and mixer noise are plotted as a function of LO power for fixed dc voltage in Fig. 3 for device A1. There are two cases of LO power which are of interest. We refer to the LO power required to maximize the (coupled) conversion efficiency as the "optimum efficiency" case. Note that the conversion efficiency and output noise peak at different LO powers, for a fixed bias voltage. However, the *mixer* noise is relatively constant near its minimum, even though the efficiency and output noise are changing very rapidly with LO power there. The second qualitative case is the "overpumped" case, where the critical current is suppressed. In that case, the output noise is drastically suppressed relative to its maximum value. The conversion efficiency is also somewhat lower than its maximum value. However, the mixer noise does not change much between the "optimum efficiency" case and the "overpumped" case. The overpumped case is of practical interest because the output noise and efficiency are less sensitive to the dc bias voltage, which will be discussed next. The general behavior indicated in Fig. 3 was observed in all the devices measured. For all the devices measured, the *mixer* noise in the overpumped case at the dc bias that minimized the mixer noise was lower than the mixer noise in the optimum efficiency case at the dc bias that minimized the mixer noise.

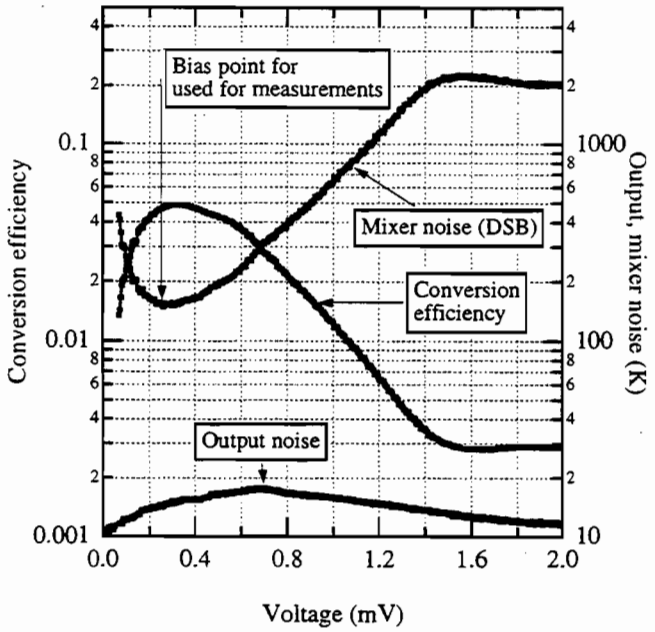

FIG. 4. Efficiency, output noise, and mixer noise vs. voltage for device B in overpumped case. IF=125-215 MHz.

2. Conversion efficiency and noise vs. dc power

In order to investigate the dependence of the conversion efficiency and noise on dc bias, the output noise and conversion efficiency were measured as a function of dc bias for two different LO powers (optimum efficiency, and overpumped) for each device. The resultant mixer noise was calculated by taking the ratio of the output noise to the conversion efficiency. The measurements were done at an IF that is low enough to be representative of the zero IF limit of the device performance. The results for a typical device (device B) are plotted in Figs. 4 and 5. The immediate conclusion in these graphs is that the mixer noise is *very low*, $\approx$ 200 to 300 K (DSB). In the overpumped case, the conversion efficiency, output noise, and mixer noise are seen to depend smoothly on the dc bias.

The results of the measurements of the frequency dependence and magnitude of the conversion efficiency and output noise are summarized in Table II. The relative spectrum of the output noise behaves similarly with frequency as the conversion efficiency, as can be seen by comparing the fitted time constant for the conversion efficiency and output noise. This implies that the 3 dB noise bandwidth is larger than the 3 dB gain bandwidth, which is also indicated by comparing the two quantities in Table II.

B. Comparison with theory

In this section, we compare the measured results of the coupled output noise and coupled conversion efficiency with the theoretical predictions presented in section II. The predicted

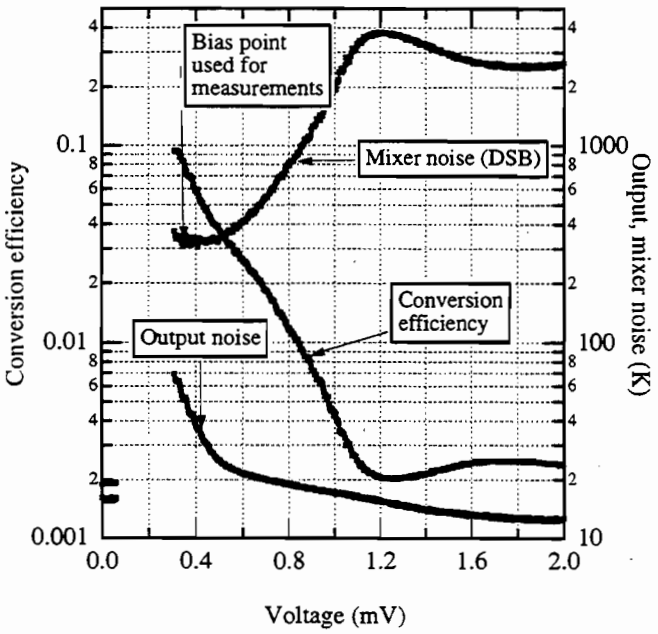

FIG. 5. Efficiency, output noise, and mixer noise vs. voltage for device B in optimum efficiency case. IF=125-215 MHz.

TABLE II. Device parameters and output noise; top half: optimum efficiency case; bottom half: overpumped case.

Dev.	L (μm)	$\eta(0)$ (dB)	$(2\pi\tau_{th})^{-1}$ (GHz) from fit of $\eta(f)$ to Eq. 2	$(2\pi\tau_{th})^{-1}$ (GHz) from fit of $T_{out}(f)$ to Eq. 13	$T_{TF}(0)$ (K) from fit of $T_{out}(f)$ to Eq. 13	T_J (K) from fit of $T_{out}(f)$ to Eq. 13	Noise BW (GHz)	$T_{mix}(0) \equiv T_{out}(0)/2\eta(0)$ (K,DSB)
A1	0.08	-5.6	$\geq$6	2.3	49	25	>6	120
A2	0.08	-	$\geq$6	-	-	-	-	-
B	0.16	-11	2.4	1.4	34	23	3.9	320
C[a]	0.24	-8	1.5	-	-	-	-	200
D	0.6	-4.1	0.3	0.13	262	19	0.73	120
E	3	-2[b]	0.08	0.13	223	8	0.75	530
A1	0.08	-7	$\geq$6	$\geq$6	-	-	>6	$\leq$100
B	0.16	-13.5	2.25	2.3	6	10	3.1	170
C	0.24	-12.7	1.5	-	-	-	-	160
D	0.6	-10.4	0.38	0.11	33	16	0.53	120
E	3	-11.7	0.064	0.045	62	7	0.16	310

[a]Device C was electrically damaged before the noise spectrum could be measured.
[b]The lowest efficiency measured was only -4 dB, but the fit returned a value of -2 dB because the lowest IF measured for this particular experiment was only 100 MHz.

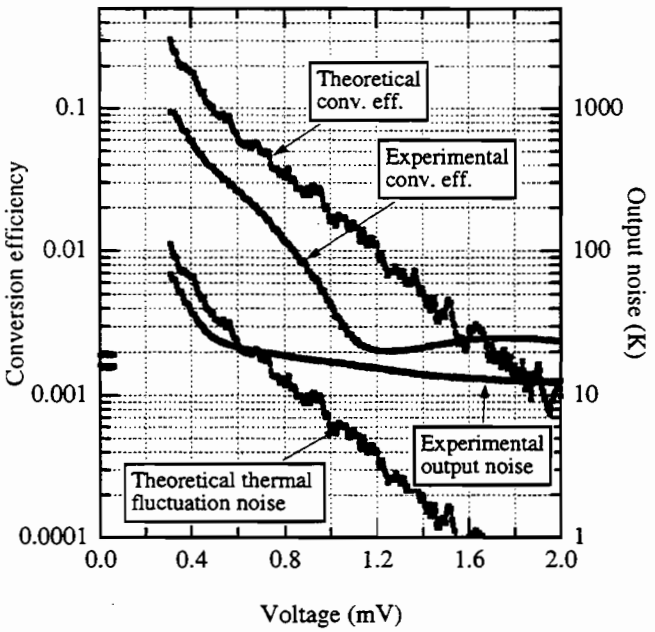

FIG. 6. Theoretical and experimental conversion efficiency and output noise for dev. B, optimum efficiency case. The predicted Johnson noise is not plotted, but is of order $T_c \approx 5.5\ K$.

conversion efficiency and output noise based on Eqs. 1 and 10 was calculated for each device by using the maximum value of dR/dT measured with small bias current and no LO power. This method is expected to predict an upper limit for η and T_{TF} since the electron temperature may not be at a point where dR/dT is maximized under operating conditions. A "local" value of dR/dT can be estimated by inferring the electron temperature from $R \equiv V_{dc}/I_{dc}$, and evaluating dR/dT at the inferred electron temperature from the measured R vs. T curve. This method was carried out for the dc bias voltages which minimized the mixer noise in both the overpumped and optimum efficiency cases. The parameters for the theoretical calculations are shown in the Appendix A, Table IV. The results of the calculated conversion efficiency based on this method are presented in Table III.

The method to determine dR/dP (which we call method 2) and hence η and T_{out} directly from the measured I-V curve was described in section II C. This procedure has also been carried out, and the resulting theoretical predictions for the conversion efficiency and noise are compared to the experimental results for a typical device (B) measured in the optimum efficiency and overpumped cases in Figs. 6- 7. Since the predictions depend on the calculated values of α and α_0, these are also plotted with the I-V curve for device B in Appendix B, Fig. 8. The results of the calculated conversion efficiency based on this second method are also in Table III for all the devices.

For devices B and C the second method gives reasonable agreement between theory and experiment. Since the length of device A is comparable to the electron-electron length ($\sqrt{D\tau_{ee}}$, with τ_{ee}^{-1} the electron-electron scattering rate), a local equilibrium temperature cannot be well defined and the simple thermal model may not apply quantitatively to this device. We have also calculated the predicted output noise and conversion efficiency as a function of dc bias using method 2 (Eq. 26) for all the devices studied in both the optimum

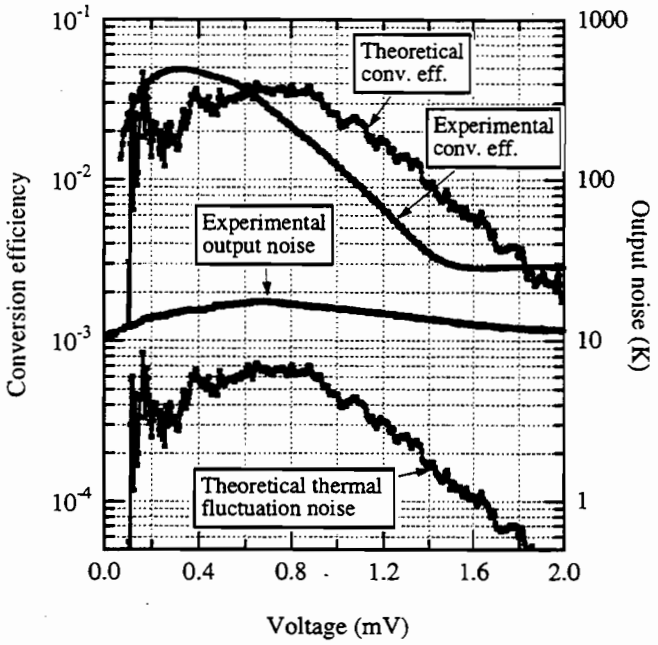

FIG. 7. Theoretical and experimental conversion efficiency and output noise for dev. B, overpumped case. The predicted Johnson noise is not plotted, but is of order $T_c \approx 5.5\ K$.

efficiency and overpumped cases [8]. We find qualitative agreement between the theoretical and experimental dc bias dependence of the output noise and efficiency for all devices except device A. However, neither method provides consistent quantitative predictions of device performance for a variety of operating conditions. Thus, device performance cannot yet be quantitatively predicted from first principles and must continue to be investigated experimentally. We find it to be excellent. Lower T_c devices made of Al may have improved performance.

ACKNOWLEDGMENTS

We thank A. Kozhevnikov for assistance with the experiments. This research was supported by the NSF and by the NASA Office of Space Science. Funding for PJB was provided by a NASA Graduate Student Fellowship as well as a Connecticut High Technology Fellowship.

APPENDIX A: DEVICE PARAMETERS

APPENDIX B: DYNAMIC AND ABSOLUTE RESISTANCE, α, AND α_0

TABLE III. Predicted and experimental conversion efficiency and output noise; top half: optimum efficiency case; bottom half: overpumped case.

Dev.	$\eta(0)$ (dB)			$T_{out}(0) = T_{TF}(0) + T_J$ (K)		
	calc. from eq. 1 max./local dR/dT used	calc. from eq. 27	expt.	calc. from eq. 10 max./local dR/dT used	calc. from eq. 28	expt.[a]
A1[b]	+1.0/-5.3	-17.5	-5.6	237.5/60.5	9	37
B	+0.2/-3.2	-7	-11	389.5/180.5	78.5	51
C	+0.7/+0.2	-9.4	-9.9	671.5/223.5	20.5	44
D[c]	+0.3/-	-0.5	-5.4	365.5/-	179.5	118
E[c]	+0.3/-	0.0	-8.6	695.5/-	409.5	105
A1[b]	+2.3/0.0	-31	-7	165.5/91.5	5.6	14
B	-2.2/-4.0	-17.2	-13.5	115.5/78.5	9	14
C	+0.7/+0.2	-13.8	-12.7	330.5/145.5	7.8	17
D[c]	0.0/-	-8.8	-10.4	92.5/-	17.5	26
E[c]	-7.0/-	-3.7	-20	42.5/-	83.5	10

[a]A value of 5.5 K was assumed for T_J in the theoretical prediction.
[b]The output noise for device A quoted in this table was measured under slightly different operating conditions than that plotted in Fig. 1.
[c]The low frequency limit of the noise and efficiency is not well-determined for devices D and E, so the experimental value at 125-175 MHz is quoted in this table.

TABLE IV. Device parameters; top half: optimum efficiency case; bottom half: overpumped case

Dev.	V_{dc} (mV)	P_{dc} (nW)	P_{LO} (nW)	dR/dT (Ω/K) loc./max.	G[a] (nW/K) Exp.(thy.)	α_0	α	η_{IF}
A1	0.45	9	13	68/140	40 (29)	0.16	0.06	0.86
B	0.35	5.5	5	135/200	30(20)	0.56	0.22	0.85
C	0.46	6.4	8	144/250	-(17)	0.41	0.086	0.95
D	0.38	5.6	15	-/250 [b]	44(-)	0.66	0.24	0.87
E	0.65	39	85	-/250	520(-)	0.71	0.46	0.58
A1	0.5	9	26	103/140	40 (29)	-0.025	-0.007	0.92
B	0.25	2.3	10	163/200	30(20)	0.095	0.028	0.92
C	0.4	4.3	16	164/250	-(17)	0.15	0.021	0.98
D	0.23	1.9	30	-/250	48(-)	0.13	0.037	0.92
E	0.2	2.9	170	-/250	520(-)	0.13	0.076	0.68

[a]Measured value at 6 K or 6.5 K extrapolated to 5.5 K. (Theoretical value calculated using $\mathcal{L}T/(R_N/12)$.) G was determined experimentally using noise thermometry measurements in the normal state.
[b]Not actually measured. Estimated based on device C, which has the same normal state resistance as devices D,E.

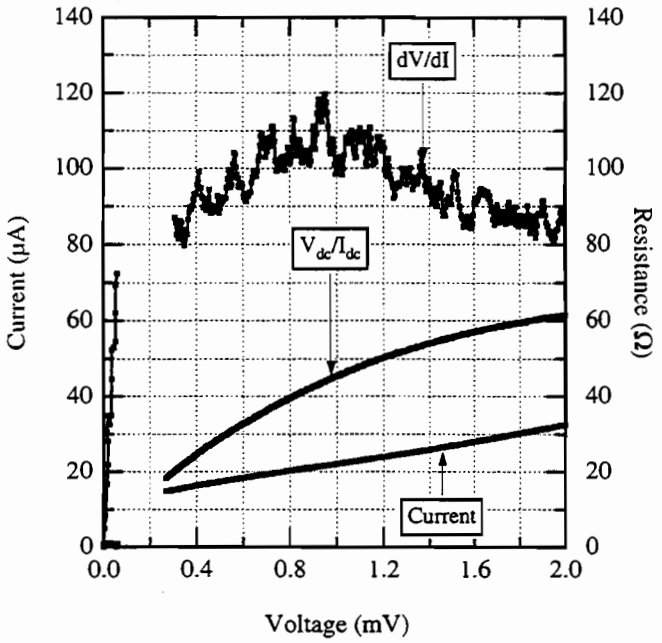

FIG. 8. IV curve, dynamic and absolute resistance for device B, optimum efficiency case.

[1] J. Kawamura, R. Blundell, C. Y. Tong, G. Gol'tsman, E. Gershenzon, and B. Voronov, Applied Physics Letters **70**, 1619 (1997).

[2] A. Skalare, W. R. McGrath, B. Bumble, H. G. LeDuc, P. J. Burke, A. A. Verheijen, R. J. Schoelkopf, and D. E. Prober, Applied Physics Letters **68**, 1558 (1996).

[3] A. Skalare, W. McGrath, B. Bumble, and H. G. LeDuc, IEEE Transactions on Applied Superconductivity **7**, 3568 (1997).

[4] B. S. Karasik, M. C. Gaidis, W. R. McGrath, B. Bumble, and H. G. LeDuc, Applied Physics Letters **71**, 1567 (1997).

[5] D. E. Prober, Applied Physics Letters **62**, 2119 (1993).

[6] P. J. Burke, R. J. Schoelkopf, D. E. Prober, A. Skalare, W. R. McGrath, B. Bumble, and H. G. LeDuc, Applied Physics Letters **68**, 3344 (1996).

[7] P. J. Burke, R. J. Schoelkopf, D. E. Prober, A. Skalare, B. S. Karasik, M. C. Gaidis, W. R. McGrath, B. Bumble, and H. G. LeDuc, Applied Physics Letters **72**, 1516 (1998).

[8] P. J. Burke, Ph.D. thesis, Yale University, 1997, available from authors.

[9] P. J. Burke, R. J. Schoelkopf, D. E. Prober, A. Skalare, B. Karasik, M. Gaidis, W. McGrath, B. Bumble, and H. LeDuc, (1998), to be submitted to Journal of Applied Physics (in preparation).

[10] F. Arams, C. Allen, B. Peyton, and E. Sard, Proceedings of the IEEE **54**, 612 (1966).

[11] H. Ekström, B. Karasik, E. Kollberg, and K. Yngvesson, IEEE Transactions on Microwave Theory and Techniques **43**, 938 (1995).

[12] B. Karasik and A. Elantev, in *Proceedings of the 6th Internation Symposium on Space Terahertz Technology*, edited by J. Zmuidzinas and G. Rebiez (CalTech, Pasadena, CA, 1995), pp. 229–246. See Ref. [24].

[13] D. W. Floet, J. Baselmans, J. Gao, and T. Klapwijk, in *Proceedings of the 9th International Symposium on Space Terahertz Technology*, edited by W. McGrath (Caltech, Pasadena, CA, 1998).

[14] J. C. Mather, Applied Optics **21**, 1125 (1982).
[15] E. Gershenzon, M. Gershenzon, G. Gol'tsman, A. M. Lyul'kin, A. Semenov, and A. Sergeev, Soviet Physics: Technical Physics **34**, 195 (1989).
[16] A. Mittal, 1995, personal communication.
[17] M. J. M. de Jong, Ph.D. thesis, Leiden University, 1995.
[18] A. Skalare, 1994, personal communication.
[19] L. D. Landau and E. M. Lifshitz, *Statistical Physics Part 2* (Pergamon, Oxford, 1980).
[20] K. M. van Vliet and J. R. Fassett, in *Fluctuation Phenomena in Solids* (Academic Press, New York, 1965), Chap. Flucuations Due to Electronic Transitions and Transport in Solids.
[21] R. F. Voss and J. Clarke, Physical Review B **13**, 556 (1976).
[22] E. Gershenzon, M. Gershenzon, G. Gol'tsman, Lyul'kin, A. Semenov, and A. Sergeev, Journal of Experimental and Theoretical Physics **70**, 505 (1990).
[23] B. Bumble and H. G. LeDuc, IEEE Transactions on Applied Superconductivity **7**, 3560 (1997).
[24] in *Proceedings of the 6th Internation Symposium on Space Terahertz Technology*, edited by J. Zmuidzinas and G. Rebiez (CalTech, Pasadena, CA, 1995).